ACS APPLIED MATERIALS & INTERFACES

Research Article

www.acsami.org

(Ag,Cu)−Ta−O Ternaries As High-Temperature Solid-Lubricant Coatings

Hongyu Gao,[†] Alberto Otero-de-la-Roza,[‡] Jingjing Gu,[§] D'Arcy Stone,[§] Samir M. Aouadi,[§] Erin R. Johnson,[∥,⊥] and Ashlie Martini*[,†]

[†]School of Engineering, University of California Merced, 5200 North Lake Road, Merced, California 95343, United States

[‡]National Institute for Nanotechnology, National Research Council of Canada, 11421 Saskatchewan Drive, Edmonton, Alberta T6G 2M9, Canada

[§]Department of Materials Science and Engineering, University of North Texas, Denton, Texas 76207, United States

[∥]Department of Chemistry, Dalhousie University, 6274 Coburg Road, Halifax, Nova Scotia B3H 4R2, Canada

[⊥]Chemistry and Chemical Biology, School of Natural Sciences, University of California Merced, 5200 North Lake Road, Merced, California 95343, United States

ABSTRACT: Ternary oxides have gained increasing attention due to their potential use as solid lubricants at elevated temperatures. In this work, the tribological properties of three ternary oxides—$AgTaO_3$, $CuTaO_3$, and $CuTa_2O_6$—were studied using a combination of density-functional theory (DFT), molecular dynamics (MD) simulations with newly developed empirical potential parameters, and experimental measurements ($AgTaO_3$ and $CuTa_2O_6$ only). Our results show that the MD-predicted friction force follows the trend $AgTaO_3$ < $CuTaO_3$ < $CuTa_2O_6$, which is consistent with the experimentally measured coefficients of friction. The wear performance from both MD and experiment exhibits the opposite trend, with $CuTa_2O_6$ providing the best resistance to wear. The sliding mechanisms are investigated using experimental characterization of the film composition after sliding, quantification of Ag or Cu cluster formation at the interface during the evolution of the film in MD, and DFT energy barriers for atom migration on the material surface. All our observations are consistent with the hypothesis that the formation of metal (or metal oxide) clusters on the surface are responsible for the friction and wear behavior of these materials.

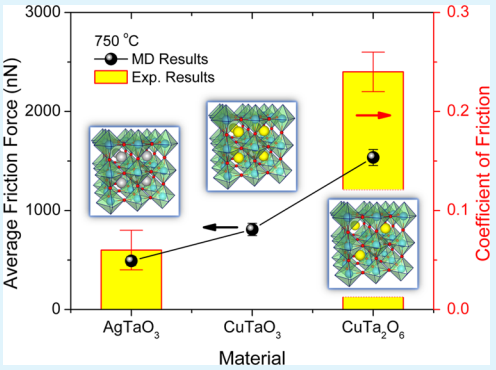

KEYWORDS: *solid lubricants, high temperature, ternary metal oxides, silver tantalate, copper tantalate, friction, wear*

1. INTRODUCTION

Lubricants are used in various engineering applications to control friction and wear. They extend the service lifetime of a sliding contact system and increase its efficiency.[1−5] In extreme working environments (e.g., vacuum or high temperature), solid lubricant coatings are often used because the low vapor pressure of solids prevents the degradation of system components caused by sublimation.[3,4] Most conventional solid lubricants, such as graphite and MoS_2, fail at elevated temperatures (>≈300 °C) because temperature-induced oxidation and the associated irreversible chemical changes result in a failure to provide the desired lubricity.[2,3,6] Considering the shortage of available candidates for high-temperature applications, developing effective solid lubricants that remain thermally stable and lubricious over a wide range of temperatures is imperative.

Oxide-based materials are promising lubricants for high-temperature applications due to their structural and chemical inertness.[4] Ternary metal oxides, including Zn(Pb)−W-(Mo,Ti)−O, Ca(Ba,Sr)−S−O, and Ag−Ta(V,Mo)−O, have been explored recently due to their low friction at high temperature.[4,7−12] Our own previous work focused on silver tantalate ($AgTaO_3$), which possesses a layer-like structure; can form a soft, metallic (silver) phase when subjected to sliding; and is highly resistant to oxidation.[12,13] The coefficient of friction (CoF) for $AgTaO_3$ was reported to decrease with temperature down to 0.06 at 750 °C.[12,14] This result was attributed to the thermal and shear-induced surface reconstruction, in which a mechanically mixed layer, including nanocrystalline Ag, Ta_2O_5, and $AgTaO_3$ phases, was observed to form at the sliding interface.[15] It was proposed that the aggregated silver, in the form of "clusters", facilitates sliding and is responsible for the low friction at the sliding interface.[14−16] However, the high mobility of silver suggests that it will also diffuse rapidly on the surface, leading to the relatively low resistance to wear observed for $AgTaO_3$. Furthermore, dispersed Ag particles have been reported to migrate and cause system failure in various high temperature components.[17]

Received: April 23, 2015
Accepted: June 24, 2015
Published: June 24, 2015

DOI: 10.1021/acsami.5b03543
ACS Appl. Mater. Interfaces 2015, 7, 15422−15429

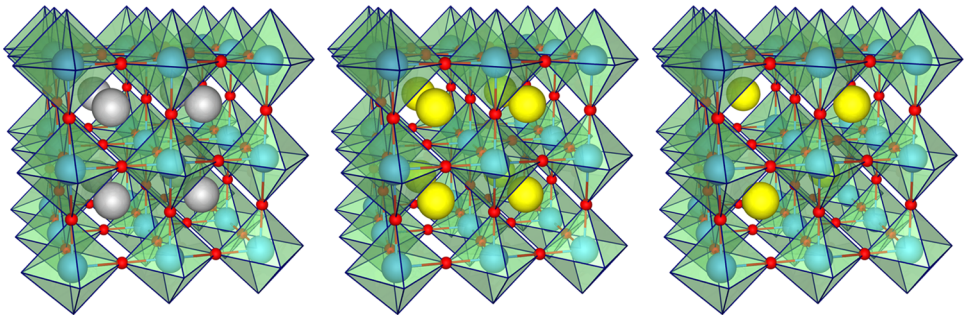

Figure 1. Structures of the (left) $AgTaO_3$, (middle) $CuTaO_3$, and (right) $CuTa_2O_6$ perovskite-like crystals; (blue) Ta, (red) O, (yellow) Cu, and (gray) Ag.

Given the relatively poor wear performance of $AgTaO_3$ and the issues associated with Ag particle migration, we have been exploring alternatives to obtain both low friction and high wear resistance. A potential candidate is a Cu−Ta−O ternary oxide because (1) both Cu and Ag are soft metals that have been used as dopants to improve tribological performance of various coating materials;[18−22] (2) Cu-based oxides have been used as high-temperature solid lubricants;[8] and (3) Cu and Ag belong to the same group of elements, so similar material properties are expected (e.g., the substitution of Cu in $Ag(Nb_xTa_{1-x})O_3$ has been performed to study the composition dependence of dielectric properties[23]). From a practical perspective, the fairly reasonable market price of Cu could render it more competitive for potential industrial applications.[24]

In this study, we focus on two Cu−Ta−O ternaries, $CuTaO_3$ and $CuTa_2O_6$, and contrast their performance with $AgTaO_3$. The structures of $AgTaO_3$, $CuTaO_3$, and $CuTa_2O_6$ are shown in Figure 1. $CuTaO_3$ was considered because it shares the same perovskite structure with $AgTaO_3$. The comparison between $CuTaO_3$ and $AgTaO_3$ will enable us to isolate the effect of the metal on the tribological performance. However, from an experimental perspective, $CuTaO_3$ is not practical because it cannot be synthesized at atmospheric pressure.[25] Therefore, $CuTaO_3$ is studied in this work using only simulations. The experiments focus on $CuTa_2O_6$, which can be prepared relatively easily. This material also has a perovskite-like structure but with alternating vacancies at the Cu sites. Additionally, a recent study showed that the frictional properties of $Ag_2Ta_4O_{11}$ differed from those of $AgTaO_3$,[12] which suggests that $CuTa_2O_6$ and $CuTaO_3$ may also have significantly different tribological properties and that tuning of coating performance may be achieved by controlling the noble-metal content of the coating during deposition.

In this work, a combination of three approaches—experiment, molecular dynamics (MD) simulation, and density-functional theory (DFT)—was used to explore and compare the tribological performance of (Ag,Cu)−Ta−O materials. Experimentally, $CuTa_2O_6$ coatings were tribotested at elevated temperatures up to 750 °C, followed by analysis of the elemental compositions and mapping of the wear track. To complement the experiments, MD simulations were performed using newly developed empirical potential parameters fit to DFT results for each Cu−Ta−O ternary oxide. The computationally predicted and experimentally measured friction and wear properties were compared with those of $AgTaO_3$. Results were analyzed in terms of the underlying sliding mechanisms with a focus on the formation of Ag/Cu clusters at the interface that can facilitate sliding. This mechanism was further investigated using DFT calculations of the energy barriers for Cu or Ag migrating on the material surfaces.

2. METHODOLOGY

2.1. Density-Functional Theory. The DFT calculations for the model potential fitting were performed using the pseudopotentials/plane-waves approach and the Projected Augmented-Wave (PAW) framework[26] with the Vienna Ab initio simulation package (VASP) program.[27,28] The cell lengths and elastic constants for all crystals were obtained using the local density approximation (LDA) functional, and the cohesive energies were calculated using the Perdew−Burke−Ernzerhof (PBE) functional.[29] Cubic cells were used for both $CuTaO_3$ ($Z = 1$) and $CuTa_2O_6$ ($Z = 4$). The plane-wave cutoff in all cases was 520 eV, with a 0.05 eV smearing parameter. Regular $14 \times 14 \times 14$ and $6 \times 6 \times 6$ k-point grids were used for $CuTaO_3$ and $CuTa_2O_6$, respectively.

Additional DFT calculations were carried out to investigate the sliding behavior of Cu on the CuO-terminated surface of $CuTaO_3$. Centrosymmetric slab models for this surface were built using three cubic $CuTaO_3$ unit cells and a total cell length in the direction perpendicular to the slab of 80 bohr (50.7 bohr vacuum). The same parameters as in the bulk calculations were used, except that in this case we employed the Perdew−Burke−Ernzerhof (PBE) functional[29] and a $6 \times 6 \times 6$ k-point grid.

2.2. Molecular Dynamics Simulation. *2.2.1. Potential Parameter Fitting.* Potential parameters for the ternary Cu−Ta−O oxide were developed based on the Modified Embedded-Atom Method (MEAM) formalism,[30] which has been successfully used to reproduce material properties of $AgTaO_3$.[31] MEAM parameters for pure Cu, Ta, and O were taken from ref. 30 and are given in Table A.1 of the Appendix. For the binary oxides, parameters were fitted based on a B1 structure, consistent with our previous fitting of the Ag−O and Ta−O binaries.[31] The relative density (ρ_0), exponential decay factor (α_{edf}), and screening parameters (C_{min} and C_{max}) for Cu−O were determined based on the structural and elastic properties predicted by DFT calculations. Next, the binary parameters were used in the fitting process for the ternary oxide, where additional potential parameters (i.e., parameters for the immiscible binary Cu−Ta and ternary Cu−Ta−O) were adjusted such that the empirical potential reproduced the DFT-predicted lattice constants, angles, elastic constants, and cohesive energy of the Cu−Ta−O compounds. Due to the differences in the chemical and mechanical properties of $CuTaO_3$ and $CuTa_2O_6$, two separate sets of potential parameters were fitted to better describe these two materials. Detailed information about the fitting process can be found in ref. 31. The LAMMPS simulation software[32] was used in the fitting process and in the sliding models discussed in the next section.

Table 1 shows the MD- and DFT-predicted structural and elastic properties of $CuTaO_3$ and $CuTa_2O_6$. The mean absolute percent differences between MD and DFT results (assigning equivalent weighting factors to each property) were 1.32 and 4.11% for $CuTaO_3$ and $CuTa_2O_6$, respectively. The final potential parameters for the two materials are given in Table A.2 of the Appendix.

To verify the validity of those parameters, we compared the energy-volume curve obtained using MD with our DFT calculations (Figure 2).

DOI: 10.1021/acsami.5b03543
ACS Appl. Mater. Interfaces 2015, 7, 15422−15429

Table 1. MD- and DFT-Predicted Structural Properties of $CuTaO_3$ and $CuTa_2O_6$

property		$CuTaO_3$		$CuTa_2O_6$	
		MEAM	DFT	MEAM	DFT
cell lengths (Å)	$a/b/c$	3.90	3.90	7.61	7.45
cell angles (deg)	$\alpha/\beta/\gamma$	90.00	90.00	90.00	90.00
cohesive energy (eV)	E_c	6.20	6.20	6.97	6.73
elastic constants (GPa)	C_{11}	450.83	503.49	426.32	431.43
	C_{12}	104.48	104.47	75.04	79.20

The results show that, within 20% of the equilibrium volume, the relative energies of both $CuTaO_3$ and $CuTa_2O_6$ are well-captured by the potentials. In addition, the MD-predicted thermal expansion coefficient for $CuTa_2O_6$ at temperatures between 200 and 1200 K is 3.73×10^{-6} K^{-1}, which is comparable to the experimental measurement of 8.0×10^{-6} K^{-1}.[33]

2.2.2. Sliding Models. Using the newly fitted MEAM parameters reported in the previous section, two sliding models were created to study the friction and wear behavior of Cu−Ta−O: (1) plate-on-plate and (2) ball-on-plate. These models are shown in Figure 3. Model 1 facilitates calculation of the average friction force and analysis of the film reconstruction during sliding, while model 2 is based on the experimental setup and enables characterization of material transfer and wear. Simulations with these two models were performed for each of the three materials: $AgTaO_3$, $CuTaO_3$, and $CuTa_2O_6$.

The dimensions of the tribofilms (i.e., the bottom plate) for all three materials were $9.7 \times 2.2 \times 11.9$ and $16.4 \times 11.9 \times 3.7$ nm^3 for Models 1 and 2, respectively. In Model 2, the ball was assigned a radius of 2.5 nm. In each model, the atoms in the top plate/ball acted as a rigid body during sliding, and the positions of the atoms in the bottommost layer of the film were fixed. The plate/ball slid laterally at a constant speed of 10 m/s with a time step of 0.5 fs. Periodic boundary conditions were applied in the sliding plane; in the direction perpendicular to that plane, atoms were confined by the rigid boundaries. Normal loads of 1000 and 300 nN were uniformly distributed on the rigid plate (in Model 1) and ball (in Model 2), respectively. Tribological simulations with the two models were performed at room temperature (RT, 27 °C) and 750 °C. The temperature was maintained using a Langevin thermostat in the canonical ensemble. The friction force was defined as the average force in the sliding direction on the plate from Model 1. The wear depth, in Model 2, was defined as the vertical distance between the equilibrated film surface and the bottom of the wear track. To quantify the evolution of the films in response to sliding, we identified Ag/Cu clusters and characterized their sizes using Model 1. A cluster was identified as a group of Ag/Cu atoms consisting of at least four atoms with each neighboring distance less than 0.25/0.20 nm, where a smaller neighbor distance criterion was used for Cu to reflect its smaller atomic radius.

2.3. Experiment. Copper tantalate coatings were produced on mechanically polished Inconel 718 substrates using an ATC 1500 unbalanced magnetron sputtering chamber (AJA International, North Scituate, MA). Sample preparation consisted of cleaning the substrates ultrasonically in acetone and methanol for 15 min, rinsing them in deionized water, and drying them using compressed nitrogen. The source materials consisted of elemental targets (Φ = 5 cm) of Ta (99.98 %) and Ag (99.997% purity) acquired from Plasmaterials, Inc. (Livermore, CA). After evacuation of the sputtering system to a base pressure $<10^{-4}$ Pa, coatings were manufactured in a mixed atmosphere of Ar (99.999%) and O_2 (99.99%) with partial pressures of 0.70 and 0.30 Pa, respectively. Substrates were held at a temperature of 350 °C and a bias potential of −100 V while being rotated about their polar axis at a speed of 50 rpm. A thin Ta layer was deposited for the initial 5 min to enhance adhesion of the coating to the substrate. Thin films of Cu−Ta−O were then deposited for 3 h, which corresponds to a total thickness of 2 μm. Power settings to the Ta and Cu targets were 200 and 10 W, respectively.

X-ray diffraction (XRD) patterns before and after tribotesting were acquired using a GBC MMA diffractometer equipped with a Cu Kα radiation source to evaluate the structural properties of the films. Wear testing of these films was carried out under a load of 2 N using a Nanovea ball-on-disk tribotester (Microphotonics, Inc., Irvine, CA) at 750 °C (heating stage temperature) in atmospheric conditions (relative humidity of 60 ± 5%) with a sliding speed of 0.11 m/s and a total sliding distance of 10 m (corresponding to more than 10 000 revolutions). The tests were performed at 3.33 Hz using a 6 mm diameter Si_3N_4 ball, because it is the material of choice in high-temperature hybrid bearing assemblies. These loads correspond to initial mean Hertzian contact stresses of 0.5, 0.6, 0.8, and 1.0 GPa, respectively. All test conditions were the same as those under which previous testing of $AgTaO_3$ was performed.[14−16,34] Three sliding tests were performed at each temperature: the elemental compositions were determined for the material as-deposited and after tribotesting, inside and outside the wear track, using a Model 670xi Scanning Auger Nanoprobe (SAN). The composition of the as-deposited film was found to be 12 at. % Cu, 25 at. % Ta, and 63 at. % O.

Figure 4 shows XRD patterns for the films before wear testing at 750 °C. The patterns revealed that the films consisted of $CuTa_2O_6$ (perovskite crystal structure). Much weaker peaks that correspond to $TaO_{1.06}$ and $Ta_{7.3}O_{11.4}$ were also observed in these patterns. Interestingly, the formation of CuO was detected after wear testing at 750 °C. Our attempt to create the $CuTaO_3$ phase by varying power to the targets, substrate temperature (from RT to 600 °C), and substrate bias voltage (from floating to 160 V) did not result in its formation. This

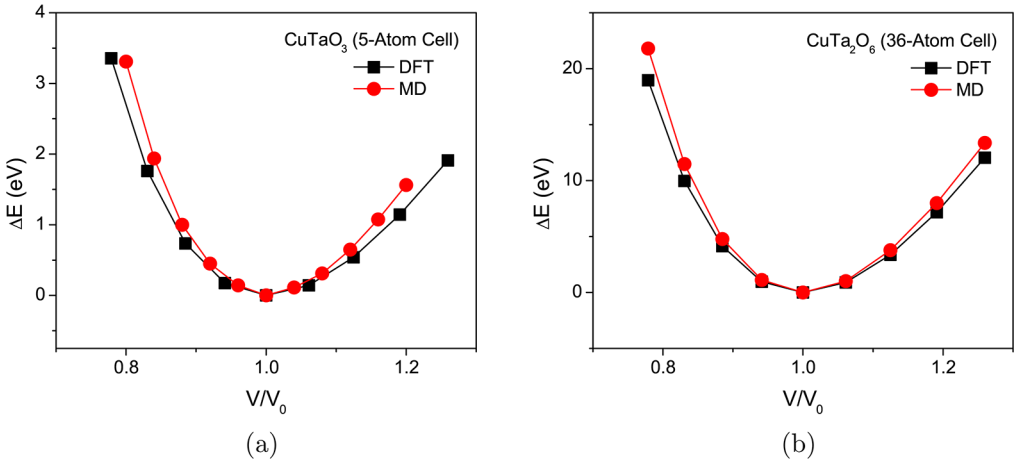

Figure 2. Volume-dependence of the energy for (a) $CuTaO_3$ and (b) $CuTa_2O_6$ from MD and DFT. ΔE is the energy relative to the equilibrium structure with volume V_0.

DOI: 10.1021/acsami.5b03543
ACS Appl. Mater. Interfaces 2015, 7, 15422−15429

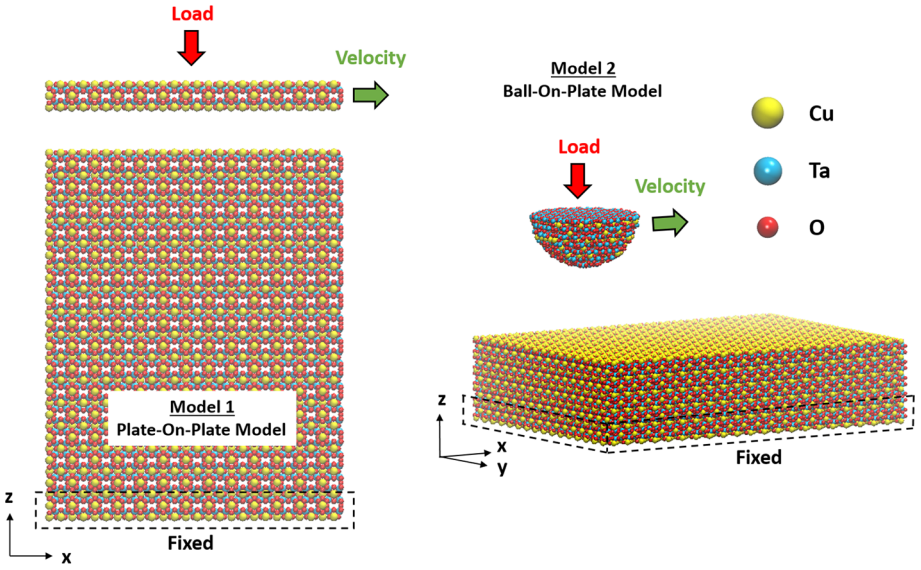

Figure 3. Initial configurations of the two MD simulation models, shown here for $CuTa_2O_6$.

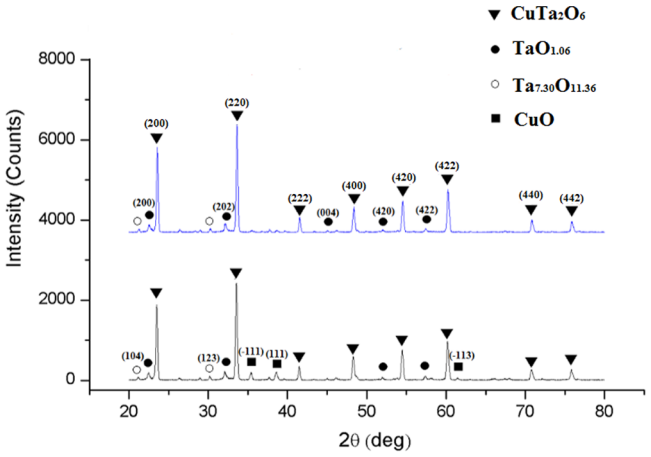

Figure 4. Representative XRD pattern of a sputtered Cu−Ta−O coating (top) before and (bottom) after wear testing at 750 °C.

is consistent with a report in the literature that bulk $CuTaO_3$ cannot be produced except at high pressures.[25]

3. RESULTS

3.1. Friction. Figure 5a shows the average friction force from MD (Model 1) for $AgTaO_3$, $CuTaO_3$, and $CuTa_2O_6$ films, and the experimental coefficients of friction for $AgTaO_3$ and $CuTa_2O_6$ films, measured at 750 °C. The friction trends from MD and experiment are in agreement:

$$f^{MD\&Exp}_{AgTaO_3} < f^{MD}_{CuTaO_3} < f^{MD\&Exp}_{CuTa_2O_6}$$

Note that the friction results from MD and experiment can not be quantitatively compared due to the inherent size-scale difference between the two techniques, where contact area and applied load in MD are orders of magnitude smaller than those in experiment. Also, in MD, strong surface adhesion at the nanoscale tends to result in a larger CoF at the sliding interface.[35] However, the ratios of the friction forces and CoFs for $AgTaO_3$ and $CuTa_2O_6$ can be directly compared, and both experiment and simulation yield

$$3 < f_{CuTa_2O_6}/f_{AgTaO_3} < 4.5$$

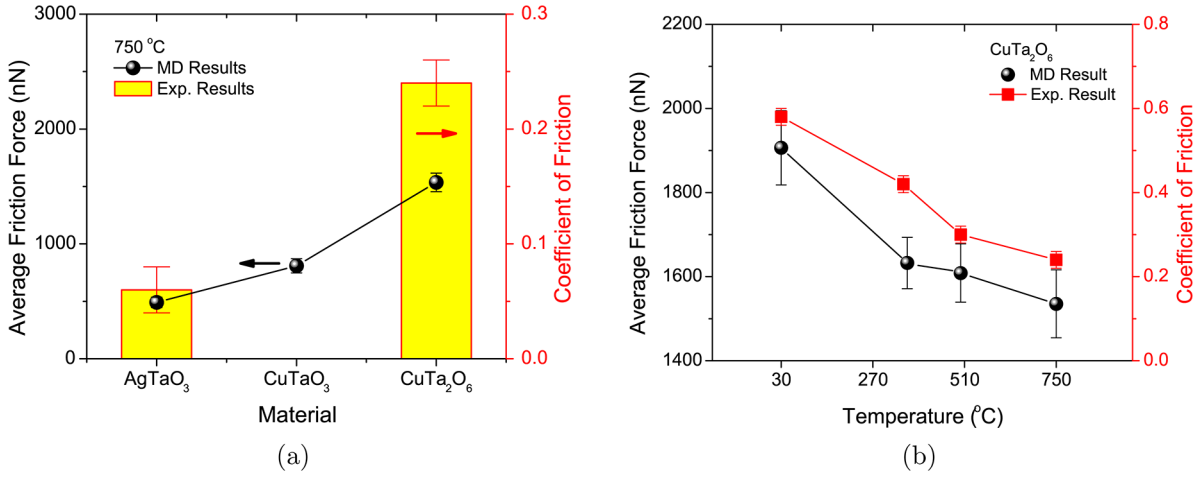

Figure 5. Friction from MD and experiment as functions of (a) material (i.e., $AgTaO_3$, $CuTaO_3$, and $CuTa_2O_6$ in MD; and $AgTaO_3$ and $CuTa_2O_6$ in experiment) at 750 °C, and (b) temperature (i.e., RT, 350, 500, and 750 °C) for $CuTa_2O_6$.

DOI: 10.1021/acsami.5b03543
ACS Appl. Mater. Interfaces 2015, 7, 15422−15429

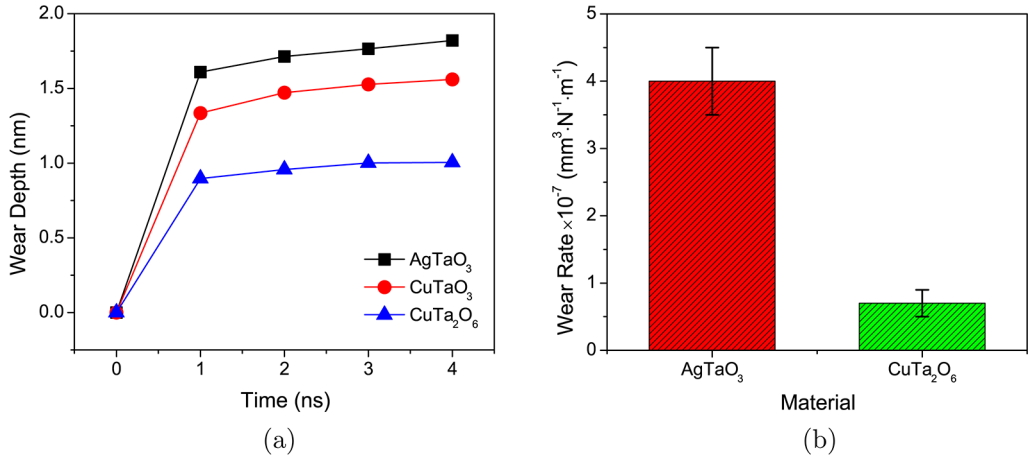

Figure 6. Wear performance of (Ag,Cu)−Ta−O at 750 °C: (a) MD-predicted wear depth and (b) experimentally measured wear rate.

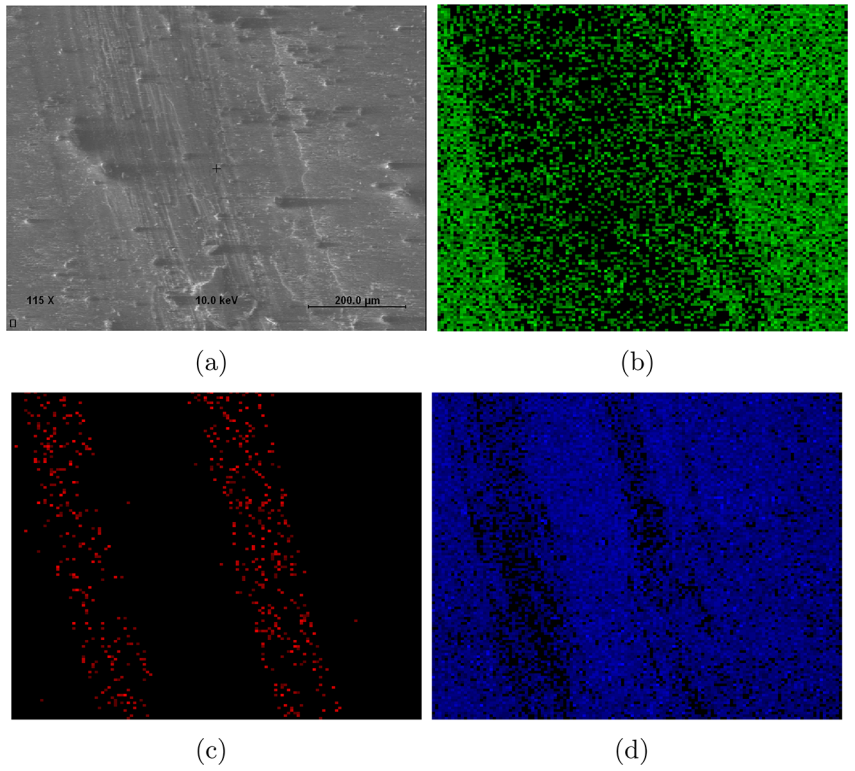

Figure 7. Characterization of a selected area of the wear track after tribotesting at 750 °C. (a) SEM image and elemental mapping of (b) copper, (c) tantalum, and (d) oxygen.

It was previously shown that the CoF of $AgTaO_3$ decreases with temperature.[14−16] The effect of temperature on friction for $CuTa_2O_6$ with both MD and experiment is shown in Figure 5b. Friction decreases with increasing temperature, exhibiting the same trend as $AgTaO_3$.

3.2. Wear. To quantify the wear performance of these materials, the MD ball-on-plate model (Model 2) was used because it allows the removal of atoms from the wear track so wear depth can be measured. Figure 6a shows that the wear depth for each material at 750 °C increases significantly at the beginning of sliding (run-in) and then approaches a steady state. The wear depth varies as

$$d_{AgTaO_3} > d_{CuTaO_3} > d_{CuTa_2O_6}$$

which is opposite to the friction trend. The experimentally measured wear rates at the same temperature, shown in Figure 6b, exhibit the same trend as that from MD, indicating that $AgTaO_3$ is more easily removed from the wear track than $CuTa_2O_6$.

4. DISCUSSION

The MD and experimental observations of opposing friction and wear trends suggest that all three materials share similar sliding mechanisms. In our previous studies,[14−16,34] we proposed that the CoF and the wear rate are determined by the ability of the monovalent metal (in this case, Ag or Cu) to migrate to the surface and agglomerate into soft metallic clusters. In this section, we investigate the ability of this mechanism to explain the observed trends. This was done with analyses of: (a) surface

DOI: 10.1021/acsami.5b03543
ACS Appl. Mater. Interfaces 2015, 7, 15422−15429

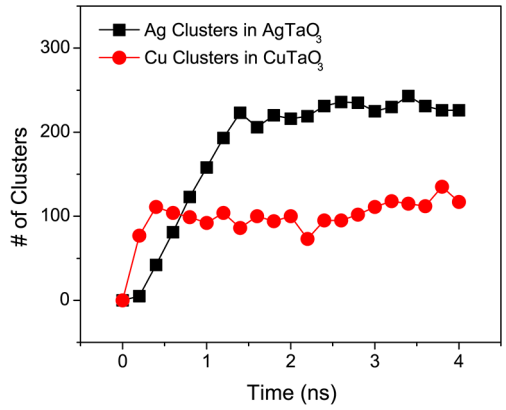

Figure 8. Number of Ag/Cu clusters in at the sliding interface from MD simulations of $AgTaO_3$ and $CuTaO_3$ at 750 °C as a function time.

elemental mapping from experiment, (b) Ag/Cu clustering at the interface in MD, and (c) Ag/Cu migration on the film surface using DFT were conducted.

4.1. Surface Characterization. The composition of the tribofilm is altered by the process of surface restructuring during contact sliding, which results in a change of the tribological performance of the lubricant material with increasing wear. To investigate this effect, Figure 7a shows the elemental mapping in the vicinity of the wear track in addition to a scanning electron microscope (SEM) micrograph of the selected region. The Cu content, shown in Figure 7b, was found to decrease dramatically in the wear track as a result of the sliding process; the Ta content, shown in Figure 7c, increased at the edges of the wear track. The observed elemental mapping is likely caused by formation of Cu or copper oxide clusters due to the dissociation of the $CuTa_2O_6$ phase in the wear track, in agreement with the simulations discussed in the following section. This ternary phase dissociation was less pronounced than in the $AgTaO_3$ coatings[16] because the Cu−O bonds are stronger than the Ag−O bonds and the energy that is required to decompose $CuTa_2O_6$ into binary oxides is much higher. Finally, the presence of a transfer film was confirmed by Raman spectroscopy, which was carried out on the Si_3O_4 ball after high-temperature sliding tests. This material transfer is consistent with observations on other ternary oxide materials that we and other authors have studied.[4,5,10]

4.2. Ag/Cu Clustering. Using the MD simulations, we quantified the evolution of the materials in response to sliding with particular focus on formation of Ag and Cu clusters. In previous work,[14−16] we showed that Ag clusters were formed in the process of $AgTaO_3$ film restructuring. Figure 8 shows the number of Ag and Cu clusters formed in the $AgTaO_3$ and $CuTaO_3$ films from Model 1 at 750 °C. The two curves increase at the beginning of sliding, typical of a run-in process, and both reach a steady state after ∼1 ns. At this steady state, the number of Cu clusters was about half of that of Ag, even though the initial amount of Ag and Cu in each film was equivalent. This result indicates that, under the same sliding conditions, Cu is less likely to segregate and form clusters than Ag. Because the film lubricity largely depends on the presence of the metallic Ag/Cu phase on the surface, the formation of clusters relates to the friction result shown in Figure 5a, where $CuTaO_3$ exhibits higher friction than $AgTaO_3$. However, Ag clusters with high mobility have low wear resistance, which results in more significant wear on $AgTaO_3$ compared to $CuTaO_3$.

For $CuTa_2O_6$, the same criteria was applied to measure the number of Cu clusters. However, only a few Cu clusters were found even after the system reached a steady state (not shown). One likely reason is that the initial Cu content in $CuTa_2O_6$ is half that of Ag or Cu in the ABO_3 perovskites for the same model size. Regardless, the simulations show that Cu is less likely to form clusters in the interface than Ag. This is consistent with the experimental observation that Cu is more uniformly distributed in the wear track on $CuTa_2O_6$ than was found in a previous analysis of Ag in the wear track on $AgTaO_3$.[16]

4.3. Ag/Cu Migration. Our DFT calculations indicate that the sliding of Cu on $CuTaO_3$ is more difficult than Ag on $AgTaO_3$. Figure 9 shows the potential energy surfaces (PES) for the sliding of Cu on CuO-terminated $CuTaO_3$ and Ag on AgO-terminated $AgTaO_3$. The features of both PES are essentially the same: the energy minimum is located at the voids along the edges of the cell, and the least-stable configuration is located above the underlying metal atoms. However, the energy barriers for the migration of Cu between minima are much higher than for Ag (by roughly a factor of 3), which suggests that the formation of metal aggregates responsible for lowering friction is not as facile for $CuTaO_3$ as for $AgTaO_3$. This explains both its higher friction and its increased resistance to wear. Because $CuTa_2O_6$ is essentially isostructural to $CuTaO_3$ but with a lower Cu content,

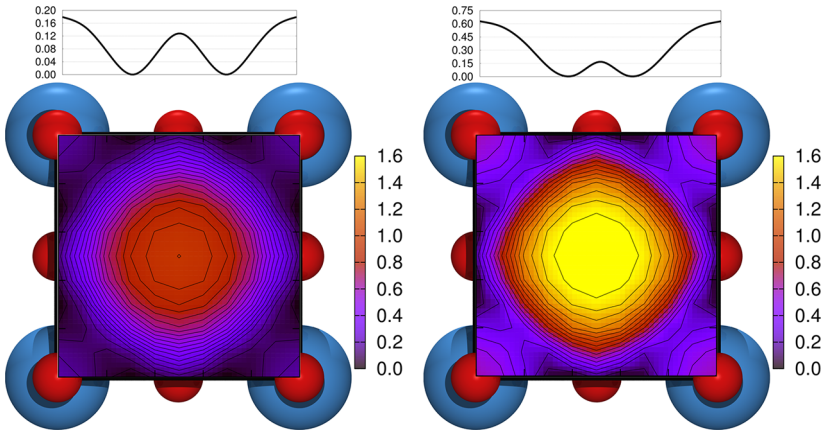

Figure 9. Potential energy surfaces for sliding (left) Ag on a AgO-terminated $AgTaO_3$ surface and (right) Cu on a CuO-terminated $CuTaO_3$ surface. The surface metal atom (Ag or Cu) occupies the center of the square. The energy scale for the colormap is the same; the units are eV. The data for $AgTaO_3$ is the same as in our previous work[16] but on a different energy scale.

DOI: 10.1021/acsami.5b03543
ACS Appl. Mater. Interfaces 2015, 7, 15422−15429

Table A.1. MEAM Parameters for Cu, Ta, and O Taken from Previous Work[30]

	E_c (eV)	a_0 (Å)	A	α_{edf}	$\beta^{(0)}$	$\beta^{(1)}$	$\beta^{(2)}$	$\beta^{(3)}$	$t^{(0)}$	$t^{(1)}$	$t^{(2)}$	$t^{(3)}$
Cu	3.54	3.62	1.07	5.11	3.63	2.20	6.00	2.20	1.00	4.37	2.49	2.95
Ta	8.09	3.30	0.99	4.90	3.71	1.00	1.00	1.00	1.00	6.09	3.35	−2.90
O	2.56	1.21	1.50	4.59	4.59	4.59	4.59	4.59	1.00	0.09	0.10	0.00

the difficulty in forming the metallic aggregates is increased by the lower availability of Cu at the surface.

5. CONCLUSION

In this work, we studied the tribological performance of three ternary oxide materials: $AgTaO_3$, $CuTaO_3$ and $CuTa_2O_6$. MEAM potential parameters for Cu−Ta−O were obtained by fitting to DFT calculations of structural and elastic properties. These potentials were then used in subsequent MD sliding simulations of $AgTaO_3$, $CuTaO_3$, and $CuTa_2O_6$. The MD predictions of friction and wear properties were compared with results of experimental tribotests on $AgTaO_3$ and $CuTa_2O_6$ films at elevated temperatures up to 750 °C. The MD and experimental trends were consistent for both friction ($AgTaO_3$ < $CuTaO_3$ < $CuTa_2O_6$) and wear ($AgTaO_3$ > $CuTaO_3$ > $CuTa_2O_6$). The wear performance was significantly improved when Ag was substituted by Cu, but at the expense of higher friction. Further analysis of the sliding mechanisms revealed that the friction increase and wear decrease could be attributed to the formation of fewer Cu clusters at the sliding interface, relative to Ag. This was corroborated by DFT calculations, which showed that the energetic barrier for migration of Cu atoms on the CuO-terminated surface of $CuTaO_3$ is considerably higher than for the equivalent sliding of Ag on $AgTaO_3$. This observation supports the hypothesis that the same friction and wear mechanisms reported for $AgTaO_3$ apply to $CuTaO_3$ and $CuTa_2O_6$, and explains the opposing friction and wear trends. Comparison of the three ternary materials enabled us to identify the key effects of the identity and relative concentration of the noble metal on tribological performance. These observations provide insights useful for developing new solid lubricants for high temperature applications.

APPENDIX

Potential Parameters

Table A.1 displayes the MEAM parameters for pure Cu, Ta, and O, taken from ref. 30. Table A.2 displays the final potential parameters for $CuTaO_3$ and $CuTa_2O_6$.

Table A.2. MEAM Parameters for the Binaries Optimized to Describe $CuTaO_3$ and $CuTa_2O_6$[a]

parameter	Cu−O	Ta−O	Cu−Ta ($CuTaO_3$)	Cu−Ta ($CuTa_2O_6$)
ρ_0^1/ρ_0^2	0.025	0.704	0.035	0.035
E_c	4.530	8.650		
r_e	2.064	2.205	5.895	7.189
α_{edf}	4.992	4.415	4.448	2.663
r_c			6.200	6.200
C_{max}			2.8	0.6
C_{min}			0.0	0.0

[a]For all binaries, the structure is B1, and the cutoff distance is 6.2 Å. For the ratio ρ_0^1/ρ_0^2, superscripts 1 and 2 indicate the first and second element listed in the binary pair, respectively.

AUTHOR INFORMATION

Corresponding Author

*E-mail: amartini@ucmerced.edu.

Notes

The authors declare no competing financial interest.

ACKNOWLEDGMENTS

A.M., H.G., J.G., D.S., and S.A. acknowledge the Air Force Office of Scientific Research (AFOSR) award No. FA9550-12-1-0221. A.O.R. thanks the Spanish Malta/Consolider Initiative (no. CSD2007-00045) and Alberta Innovates Technology Futures (AITF) for funding.

REFERENCES

(1) Donnet, C.; Erdemir, A. Historical Developments and New Trends in Tribological and Solid Lubricant Coatings. *Surf. Coat. Technol.* **2004**, *180−181*, 76−84.

(2) Scharf, T. W.; Prasad, S. V. Solid Lubricants: A Review. *J. Mater. Sci.* **2013**, *48*, 511−531.

(3) Muratore, C.; Voevodin, A. A. Chameleon Coatings: Adaptive Surfaces to Reduce Friction and Wear in Extreme Environments. *Annu. Rev. Mater. Res.* **2009**, *39*, 297−324.

(4) Aouadi, S. M.; Gao, H.; Martini, A.; Scharf, T. W.; Muratore, C. Lubricious Oxide Coatings for Extreme Temperature Applications: A Review. *Surf. Coat. Technol.* **2014**, *257*, 266−277.

(5) Zabinski, J. S.; Sanders, J. H.; Nainaparampil, J.; Prasad, S. V. Lubrication Using A Microstructurally Engineered Oxide: Performance and Mechanisms. *Tribol. Lett.* **2000**, *8*, 103−116.

(6) Scharf, T. W.; Rajendran, A.; Banerjee, R.; Sequeda, F. Growth, Structure and Friction Behavior of Titanium Doped Tungsten Disulphide (Ti-WS_2) Nanocomposite Thin Films. *Thin Solid Films* **2009**, *517*, 5666−5675.

(7) Strong, K. L.; Zabinski, J. S. Tribology of Pulsed Laser Deposited Thin Films of Cesium Oxythiomolybdate (Cs_2MoOS_3). *Thin Solid Films* **2002**, *406*, 174−184.

(8) Gulbiński, W.; Suszko, T.; Sienicki, W.; Warcholiński, B. Tribological Properties of Silver- and Copper-Doped Transition Metal Oxide Coatings. *Wear* **2003**, *254*, 129−135.

(9) Aouadi, S. M.; Paudel, Y.; Luster, B.; Stadler, S.; Kohli, P.; Muratore, C.; Hager, C.; Voevodin, A. A. Adaptive Mo_2N/MoS_2/Ag Tribological Nanocomposite Coatings for Aerospace Applications. *Tribol. Lett.* **2008**, *29*, 95−103.

(10) Aouadi, S. M.; Singh, D. P.; Stone, D. S.; Polychronopoulou, K.; Nahif, F.; Rebholz, C.; Muratore, C.; Voevodin, A. A. Adaptive VN/Ag Nanocomposite Coatings with Lubricious Behavior from 25 to 1000 °C. *Acta Mater.* **2010**, *58*, 5326−5331.

(11) Liang, X.-S.; Ouyang, J.-H.; Liu, Z.-G.; Yang, Z.-L. Friction and Wear Characteristics of $BaCr_2O_4$ Ceramics at Elevated Temperatures in Sliding Against Sintered Alumina Ball. *Tribol. Lett.* **2012**, *47*, 203−209.

(12) Stone, D. S.; Harbin, S.; Mohseni, H.; Mogonye, J.-E.; Scharf, T. W.; Muratore, C.; Voevodin, A. A.; Martini, A.; Aouadi, S. M. Lubricious Silver Tantalate Films for Extreme Temperature Applications. *Surf. Coat. Technol.* **2013**, *217*, 140−146.

(13) Stone, D. S.; Liu, J.; Singh, D. P.; Muratore, C.; Voevodin, A. A.; Mishra, S.; Rebholz, C.; Ge, Q.; Aouadi, S. M. Layered Atomic Structures of Double Oxides for Low Shear Strength at High Temperatures. *Scr. Mater.* **2010**, *62*, 735−738.

(14) Gao, H.; Stone, D. S.; Mohseni, H.; Aouadi, S. M.; Scharf, T. W.; Martini, A. Mechanistic Studies of High Temperature Friction Reduction in Silver Tantalate. *Appl. Phys. Lett.* **2013**, *102*, 121603.

DOI: 10.1021/acsami.5b03543
ACS Appl. Mater. Interfaces 2015, 7, 15422−15429

(15) Stone, D. S.; Gao, H.; Chantharangsi, C.; Paksunchai, C.; Bischof, M.; Jaeger, D.; Martini, A.; Scharf, T. W.; Aouadi, S. M. Load-Dependent High Temperature Tribological Properties of Silver Tantalate Coatings. *Surf. Coat. Technol.* **2014**, *244*, 37−44.
(16) Gao, H.; Otero-de-la-Roza, A.; Aouadi, S. M.; Martini, A.; Johnson, E. R. Chemical Basis of the Tribological Properties of $AgTaO_3$ Crystal Surfaces. *J. Phys. Chem. C* **2014**, *118*, 17577−17584.
(17) Cushen, M.; Kerry, J.; Morris, M.; Cruz-Romero, M.; Cummins, E. Migration and Exposure Assessment of Silver from A PVC Nanocomposite. *Food Chem.* **2013**, *139*, 389−397.
(18) Baker, M. A.; Kench, P. J.; Joseph, M. C.; Tsotsos, C.; Leyland, A.; Matthews, A. The Nanostructure and Mechanical Properties of PVD CrCu (N) Coatings. *Surf. Coat. Technol.* **2003**, *162*, 222−227.
(19) Gulbiński, W.; Suszko, T. Thin Films of Mo_2N/Ag Nanocomposite—the Structure, Mechanical and Tribological Properties. *Surf. Coat. Technol.* **2006**, *201*, 1469−1476.
(20) He, J. L.; Setsuhara, Y.; Shimizu, I.; Miyake, S. Structure Refinement and Hardness Enhancement of Titanium Nitride Films by Addition of Copper. *Surf. Coat. Technol.* **2001**, *137*, 38−42.
(21) Myung, H. S.; Lee, H. M.; Shaginyan, L. R.; Han, J. G. Microstructure and Mechanical Properties of Cu Doped TiN Superhard Nanocomposite Coatings. *Surf. Coat. Technol.* **2003**, *163−164*, 591−596.
(22) Han, J. G.; Myung, H. S.; Lee, H. M.; Shaginyan, L. R. Microstructure and Mechanical Properties of Ti-Ag-N and Ti-Cr-N Superhard Nanostructured Coatings. *Surf. Coat. Technol.* **2003**, *174−175*, 738−743.
(23) Duguey, S.; Lebourgeois, R.; Grattepain, C.; Heintz, J.-M.; Ganne, J.-P. Study of Copper Substitutions in $Ag(Nb_xTa_{1-x})O_3$ Solid Solutions. *J. Eur. Ceram. Soc.* **2007**, *27*, 1171−1175.
(24) Valant, M.; Axelsson, A.-K.; Alford, N. Review of $Ag(Nb,Ta)O_3$ as a Functional Material. *J. Eur. Ceram. Soc.* **2007**, *27*, 2549−2560.
(25) Sleight, A. W.; Prewitt, C. T. Preparation of $CuNbO_3$ and $CuTaO_3$ at High Pressure. *Mater. Res. Bull.* **1970**, *5*, 207−211.
(26) Blöchl, P. E. Projector Augmented-Wave Method. *Phys. Rev. B: Condens. Matter Mater. Phys.* **1994**, *50*, 17953.
(27) Kresse, G.; Furthmüller, J. Efficiency of ab-initio Total Energy Calculations for Metals and Semiconductors Using A Plane-Wave Basis Set. *Comput. Mater. Sci.* **1996**, *6*, 15−50.
(28) Kresse, G.; Furthmüller, J. Efficient Iterative Schemes for *ab initio* Total-Energy Calculations Using A Plane-Wave Basis Set. *Phys. Rev. B: Condens. Matter Mater. Phys.* **1996**, *54*, 11169−11186.
(29) Perdew, J. P.; Burke, K.; Ernzerhof, M. Generalized Gradient Approximation Made Simple. *Phys. Rev. Lett.* **1996**, *77*, 3865−3868.
(30) Baskes, M. I. Modified Embedded-Atom Potentials for Cubic Materials and Impurities. *Phys. Rev. B: Condens. Matter Mater. Phys.* **1992**, *46*, 2727−2742.
(31) Gao, H.; Otero-de-la-Roza, A.; Aouadi, S. M.; Johnson, E. R.; Martini, A. An Empirical Model for Silver Tantalate. *Modell. Simul. Mater. Sci. Eng.* **2013**, *21*, 055002.
(32) Plimpton, S. Fast Parallel Algorithms for Short-Range Molecular Dynamics. *J. Comput. Phys.* **1995**, *117*, 1−19.
(33) Longo, J. M.; Sleight, A. W. $CuTa_2O_6$−Crystal Growth and Characterization. *Mater. Res. Bull.* **1975**, *10*, 1273−1277.
(34) Stone, D. S.; Gao, H.; Chantharangsi, C.; Paksunchai, C.; Bischof, M.; Martini, A.; Aouadi, S. M. Reconstruction Mechanisms of Tantalum Oxide Coatings with Low Concentrations of Silver for High Temperature Tribological Applications. *Appl. Phys. Lett.* **2014**, *105*, 191607.
(35) Yoshizawa, H.; Chen, Y. L.; Israelachvili, J. Fundamental Mechanisms of Interfacial Friction. 1. Relation between Adhesion and Friction. *J. Phys. Chem.* **1993**, *97*, 4128−4140.

DOI: 10.1021/acsami.5b03543
ACS Appl. Mater. Interfaces 2015, 7, 15422−15429